NASA/TM—2006-214330

Foreign Object Damage in a Gas-Turbine Grade Silicon Nitride by Spherical Projectiles of Various Materials

Sung R. Choi
University of Toledo, Toledo, Ohio

Zsolt Racz
Ohio Aerospace Institute, Brook Park, Ohio

Ramakrishna T. Bhatt and David N. Brewer
Glenn Research Center, Cleveland, Ohio

September 2006

NASA STI Program . . . in Profile

Since its founding, NASA has been dedicated to the advancement of aeronautics and space science. The NASA Scientific and Technical Information (STI) program plays a key part in helping NASA maintain this important role.

The NASA STI Program operates under the auspices of the Agency Chief Information Officer. It collects, organizes, provides for archiving, and disseminates NASA's STI. The NASA STI program provides access to the NASA Aeronautics and Space Database and its public interface, the NASA Technical Reports Server, thus providing one of the largest collections of aeronautical and space science STI in the world. Results are published in both non-NASA channels and by NASA in the NASA STI Report Series, which includes the following report types:

- TECHNICAL PUBLICATION. Reports of completed research or a major significant phase of research that present the results of NASA programs and include extensive data or theoretical analysis. Includes compilations of significant scientific and technical data and information deemed to be of continuing reference value. NASA counterpart of peer-reviewed formal professional papers but has less stringent limitations on manuscript length and extent of graphic presentations.

- TECHNICAL MEMORANDUM. Scientific and technical findings that are preliminary or of specialized interest, e.g., quick release reports, working papers, and bibliographies that contain minimal annotation. Does not contain extensive analysis.

- CONTRACTOR REPORT. Scientific and technical findings by NASA-sponsored contractors and grantees.

- CONFERENCE PUBLICATION. Collected papers from scientific and technical conferences, symposia, seminars, or other meetings sponsored or cosponsored by NASA.

- SPECIAL PUBLICATION. Scientific, technical, or historical information from NASA programs, projects, and missions, often concerned with subjects having substantial public interest.

- TECHNICAL TRANSLATION. English-language translations of foreign scientific and technical material pertinent to NASA's mission.

Specialized services also include creating custom thesauri, building customized databases, organizing and publishing research results.

For more information about the NASA STI program, see the following:

- Access the NASA STI program home page at *http://www.sti.nasa.gov*

- E-mail your question via the Internet to *help@sti.nasa.gov*

- Fax your question to the NASA STI Help Desk at 301–621–0134

- Telephone the NASA STI Help Desk at 301–621–0390

- Write to:
  NASA STI Help Desk
  NASA Center for AeroSpace Information
  7121 Standard Drive
  Hanover, MD 21076–1320

NASA/TM—2006-214330

Foreign Object Damage in a Gas-Turbine Grade Silicon Nitride by Spherical Projectiles of Various Materials

Sung R. Choi
University of Toledo, Toledo, Ohio

Zsolt Racz
Ohio Aerospace Institute, Brook Park, Ohio

Ramakrishna T. Bhatt and David N. Brewer
Glenn Research Center, Cleveland, Ohio

National Aeronautics and
Space Administration

Glenn Research Center
Cleveland, Ohio 44135

September 2006

Acknowledgments

The authors are thankful to Ralph Pawlik for experimental work during the course of this study. This work was supported by the Ultra-Efficient Engine Technologies (UEET) Programs, NASA Glenn Research Center, Cleveland, Ohio.

Level of Review: This material has been technically reviewed by technical management.

Available from

NASA Center for Aerospace Information
7121 Standard Drive
Hanover, MD 21076–1320

National Technical Information Service
5285 Port Royal Road
Springfield, VA 22161

Available electronically at http://gltrs.grc.nasa.gov

Foreign Object Damage in a Gas-Turbine Grade Silicon Nitride by Spherical Projectiles of Various Materials

Sung R. Choi
University of Toledo
Toledo, Ohio 43606

Zsolt Racz
Ohio Aerospace Institute
Brook Park, Ohio 44142

Ramakrishna T. Bhatt and David N. Brewer
National Aeronautics and Space Administration
Glenn Research Center
Cleveland, Ohio 44135

Abstract

Assessments of foreign object damage (FOD) of a commercial, gas-turbine grade, in situ toughened silicon nitride ceramic (AS800, Honeywell Ceramic Components) were made using four different projectile materials at ambient temperature. AS800 flexure target specimens rigidly supported were impacted at their centers in a velocity range from 50 to 450 m/s by spherical projectiles with a diameter of 1.59 mm. Four different projectile materials were used including hardened steel, annealed steel, silicon nitride ceramic, and brass. Post-impact strength of each target specimen impacted was determined as a function of impact velocity to appraise the severity of local impact damage. For a given impact velocity, the degree of strength degradation was greatest for ceramic balls, least for brass balls, and intermediate for annealed and hardened steel balls. For steel balls, hardened projectiles yielded more significant impact damage than annealed counterparts. The most important material parameter affecting FOD was identified as hardness of projectiles. Impact load as a function of impact velocity was quasi-statically estimated based on both impact and static indentation associated data.

Introduction

Ceramics, because of their brittle nature, are susceptible to localized surface damage and/or cracking by impacting objects. It is also true that ceramic components may fail structurally even by soft particles when the kinetic energy of impacting objects exceeds certain limits. The latter case has been often found in aeroengines in which combustion products, loosened metallic particles or small ingested foreign objects cause severe damage to blade/vane components, resulting in serious structural problems. Therefore, foreign object damage (FOD) associated with particle impact needs to be considered when ceramic materials are designed for structural applications. In view of this importance, a considerable amount of work on impact damage of brittle materials by sharp particles, by "blunt" particles or by plates has been accumulated both experimentally and analytically, including the assessments of FOD for gas turbine engine applications [1–16].

In previous studies [17–20], FOD behavior of two gas-turbine grade silicon nitrides, AS800 and SN282, was determined at ambient temperature using both flexure bars and disks. Fully supported ceramic target specimens were impacted at their centers by hardened steel ball projectiles with a diameter of 1.59 mm in a velocity range from 220 to 440 m/s. AS800 silicon nitride exhibited a greater FOD resistance than SN282 counterpart. With an additional equiaxed, fine-grained silicon nitride (NC132), the key material parameter, affecting FOD most, was found to be fracture toughness of a target material: the greater fracture toughness, the greater FOD resistance [17–20]. No single crack system was involved in

impact event with increasing impact velocity, resulting in several different types of flaws associated individually or simultaneously. A fracture map was proposed to identify the occurrence of particular crack systems. The degree of damage was much more severe in thin biaxial disks than in flexure bars. It was also observed that from a structural point of view, a gas-turbine grade Sylramic SiC/SiC ceramic matrix composite (CMC) exhibited a much improved impact damage resistance over AS800 or SN282 monolithic silicon nitride [21]. All of the previous FOD work has been performed using *hardened* steel ball projectiles with a hardness of HRC ≥ 60.

The current work extends the work of the previous studies by investigates FOD behavior of a gas-turbine grade silicon nitride, AS800, in terms of the effect of projectile material. Three different materials of ball projectiles were used, including steel, silicon nitride, and brass. Two different annealing temperatures, 350 and 700 °C, were used to reduce hardness of as-received, hardened steel balls. Rigidly-supported target specimens with a flexure bar configuration were impacted at their centers at velocities ranging from 50 to 450 m/s by 1.59-mm-diameter ball projectiles. Post-impact strength of each target specimen was determined in four-point flexure as a function of projectile velocity to evaluate the severity of impact damage. Static indentation testing was also carried out to determine both the impression/ deformation of metallic balls and the indentation contact damage of target specimens by ceramic balls, from which impact load would be quasi-statically estimated with respect to impact velocity. Effect of projectile hardness on impact damage in ceramics has been explored in a previous study [15], but its aspects and approaches were different from those of this study. Some of the work presented herein has been reported previously [22].

Experimental Procedures

Target and Projectiles

Target material used in this work was a commercially available gas-pressure sintered silicon nitride, AS800 (fabricated by Honeywell Ceramic Components, Torrance, CA, 1999 vintage, gel-cast). This silicon nitride has been considered one of the strong candidate ceramics for gas-turbine applications in view of its substantially improved elevated-temperature properties. AS800 is in situ toughened silicon nitride, with microstructures tailored to achieve elongated grain structures. AS800 silicon nitride has been used at the NASA Glenn Research Center in lifing [27–29] and FOD programs [17–20]. The billets were machined into flexure target specimens measuring 3 by 4 by 25 or 50 mm, respectively, in depth, width and length in accordance with a machining procedure detailed in a test standard ASTM C 1161 (size “B”) [25]. The final finish of target specimens was completed with a 600 grit diamond wheel.

Projectile materials chosen to yield a wide range of hardness were SAE 52100 chrome steel, silicon nitride, and brass. All projectiles were spherical in shape with a diameter of 1.59 mm (= 1/16 in.). Chrome steel and silicon nitride projectiles were originally for rolling elements of bearings with grades 25 and 5, respectively. Hardened chrome steel balls were annealed at 350 or 700 °C in argon for 1h to achieve increased ductility. Values of Vickers hardness of annealed steel balls, determined with an indent load of 5 N, were 5.9±0.1 and 2.4±0.1 GPa, respectively, annealed at 350 and 700 °C, as compared with 8.2±0.2 GPa for hardened (as-received) steel balls. The silicon nitride projectile material, NBD200 (fabricated by Saint-Gobain Ceramics, East Granby, CT) was MgO doped, hot isostatically pressed (HIP), fine-grained material. Vickers microhardness of silicon nitride balls was reported to be 15.5 GPa from the manufacturer’s data. Brass ball projectiles were in grade 200 and their Vickers hardness was found to be 1.9±0.1 GPa at an indent load of 5 N. Hardness of metallic projectiles was determined with a total of five indents made on the ground-off flattened side of each individual ball for a given material/heat treatment. The basic mechanical and physical properties of target AS800 silicon nitride as well as of various projectiles used are summarized in table 1.

TABLE 1.—BASIC MECHANICAL AND PHYSICAL PROPERTIES OF TARGET AND PROJECTILE MATERIALS AT AMBIENT TEMPERATURE

Material		Elastic modulus[a] E (GPa)	Poisson's ratio,[a] ν	Density[b] ρ (g/cm^3)	Vickers hardness[c] H_v (GPa)	Flexure strength[d] (MPa)	Fracture toughness[e] K_{Ic} (MPa√m)	Manufacturer
Target	AS800 silicon nitride [18]	309	0.27	3.27	13.6±1.4	775±45	8.1±0.3	Honeywell Ceramic Comp. (Torrance, CA)
Projectiles (1.59 mm diameter)	Chrome steel (SAE 52100), hardened	[g]200	[g]0.3	7.78±0.05	8.2±0.2 (HRC≥60)	[g]2200 (tension)	---	[h]N.K
	Chrome steel (SAE 52100), 350 °C annealed	[g]200	[g]0.3	7.78±0.05	5.9±0.1	---	---	[h]N.K
	Chrome steel (SAE 52100), 700 °C annealed	[g]200	[g]0.3	7.78±0.05	2.4±0.03	---	---	[h]N.K
	Brass	[g]110	[g]0.3	8.59±0.06	1.9±0.1	[g]400 (tension)	---	TRD Specialties, Inc., (Pine Meadow, CT)
	Silicon nitride (NBD200)	[f]320	[f]0.27	3.21±0.02	[f]15.5	[f]>900	[f]>5.5	Saint Gobain Ceramics, (East Granby, CT)

[a]By the impulse excitation of vibration technique, ASTM C 1259 [23].
[b]By mass/volume method with five specimens or projectiles used.
[c]By Vickers microhardness indentation; 98 N for AS800 [ASTM C 1327 [24] and 5 N for all metals, with five indents for a specimen or projectile.
[d]By four-point flexure testing (with 20/40mm spans), ASTM C 1161 [25].
[e]By single edge precracked beam (SEPB) method, ASTM C 1421 [26].
[f]From manufacturers' data.
[g]From literature data.
[h]Manufacturer 'not known' (acquired from distributors).

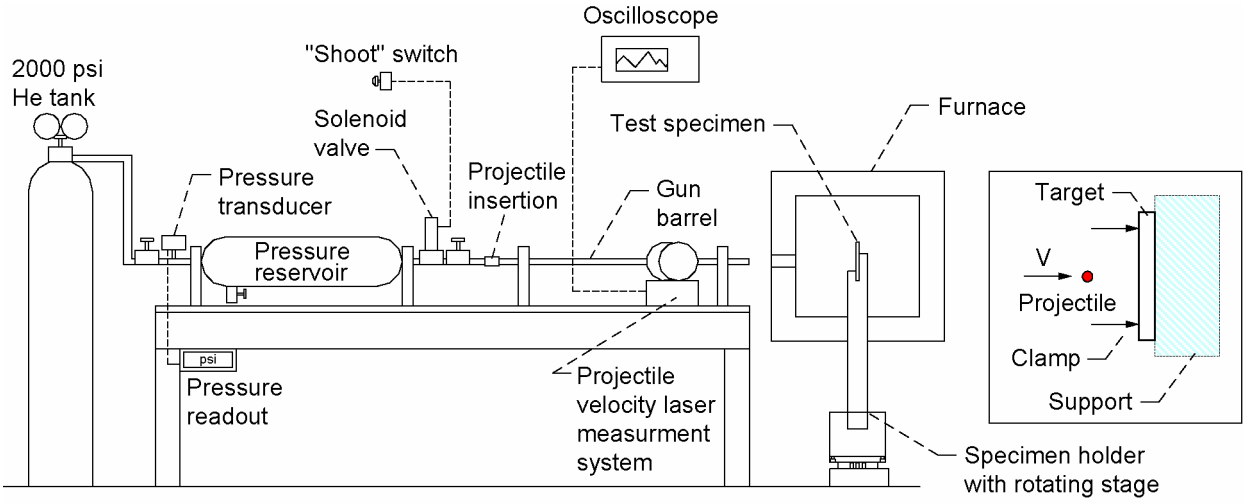

Figure 1.—Foreign object damage (FOD) test apparatus with a high-temperature furnace [18,19]. A target on a rigid support with clamps is shown in the insert.

Foreign Object Damage Testing

Foreign object damage (FOD) testing was carried out at ambient temperature using the experimental apparatus shown in figure 1. Detailed descriptions of the apparatus can be found elsewhere [17– 20]. Each projectile was inserted into a 300-mm-long gun barrel with an inner diameter of 1.59 mm. A He-gas cylinder and relief valves were used to pressurize the reservoir to a specific level, depending on

prescribed impact velocity. Upon reaching a specific level of pressure, a solenoid valve was instantaneously opened accelerating a projectile through the gun barrel to impact a target specimen. The target specimen was fully supported on a rigid steel block. Each target specimen was aligned such that the projectile impacted at the center of the 4 mm-wide side of the specimen with a normal incidence angle.

Impact velocity of each projectile was determined using two pairs of laser transmitter and receiver, incorporated with two holes in the gun barrel, as described before [18, 19]. The range of impact velocity employed in this work was from 50 to 450 m/s, depending on the type of projectiles. For a chosen projectile material, typically 5 to 10 specimens were impacted at each velocity. Projectiles were collected after impact. Impact morphologies of target specimens and projectiles were examined optically after testing. FOD testing using hardened steel ball projectiles had been conducted previously [18] and its data were used in this study.

Post-Impact Strength Testing

Strength testing for impacted target specimens was performed at ambient temperature in air to determine the severity of impact damage in four-point flexure with 20-mm inner and 40-mm outer spans (or 10-mm inner and 20-mm outer spans). Each impacted specimen was loaded in a four-point steel flexure fixture such that its impact site was subjected to tension within the inner span of the fixture. An electromechanical test frame (Model 8562, Instron, Canton, MA) was used in displacement control with an actuator speed of 0.5 mm/min. A fractographic analysis was performed after post-impact strength testing to determine failure origin, flaw configuration, and mode of fracture, etc.

Static Indentation Testing

Static indentation testing for AS800 target specimens indented with metallic and ceramic ball projectiles was conducted in an effort to estimate impact load quasi-statically. For the metallic ball projectiles, size of impression flattened was determined as a function of indent load; whereas, for the silicon nitride ball projectiles, indentation strength of target was determined as a function of indent load. The static indentation experiment was performed to determine a relationship between contact diameter and applied indent load and a relationship between indent strength and indent load with which a meaningful estimation and comparison could be made in terms of impact load and other parameters involved in projectile impact.

Static Indentation Testing With Metallic Ball Projectiles

Static indentation testing was carried out, where metallic ball projectiles - hardened and annealed steel balls and brass balls, were indented onto AS800 disks (45 mm in diameter and 2 mm in thickness and diameter). Each individual indentation load was applied (one at a time) with the respective ball indenter for about 20 s using a test frame (Type TT or 8562, Instron, Canton, MA). A total of eight indentation loads ranging from 0 to 300 N were used. The diameter of contact marked in each ball indenter upon indentation, which was easily discernable as a flattened circle of impression due to plastic deformation, was measured as a function of indentation load.

Static Indentation Testing With Silicon Nitride Ball Projectiles

Crushing Strength of Silicon Nitride Ball Projectiles

Crushing strength (or crushing load) of silicon nitride ball projectiles was determined in compression using a fixture configuration shown in figure 2. Each ball projectile was loaded against an individual AS800 flexure specimen through a mild steel nut until the projectile crushed. Polymeric thin tape was placed between the steel nut and the ceramic ball to make the ball-AS800 contact a preferential failure

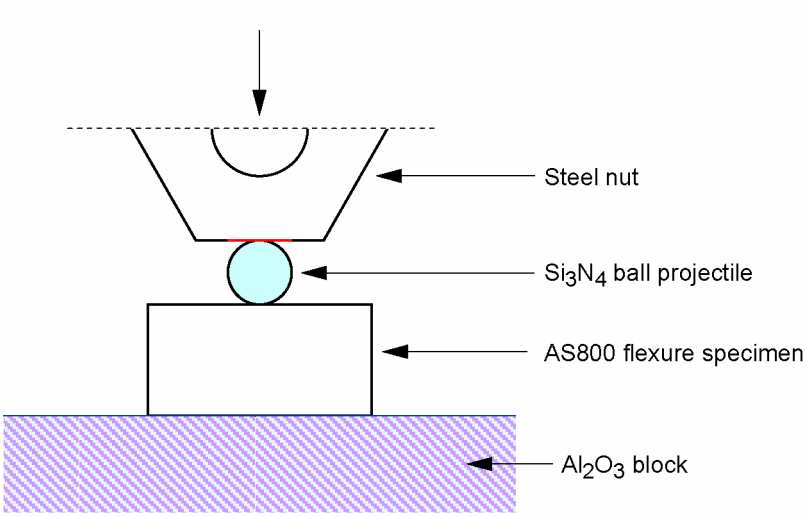

Figure 2.—Schematic of crushing test for silicon nitride ball projectiles in compression. Thin polymeric tape was inserted between loading steel nut and silicon nitride ball projectile.

site by inducing increased contact stresses therein. The electromechanical test frame was used in displacement control with an actuator speed of 0.5 mm/min. A total of seven silicon nitride ball projectiles were tested.

Indent Strength Response of AS800 Target

Indentation strength as a function of indent load was determined for AS800 flexure target specimens indented with silicon nitride ball projectiles using a test configuration similar to figure 2. Each indentation was applied in air for 20 s at the center of the 4 mm-wide side of each flexure test specimen measuring 3 by 4 by 25 mm, respectively, in depth, width and length. A total of 6 indent loads ranging from 500 to 1700 N were used. Flexure strength of indented test specimens was determined at ambient temperature in air in four-point flexure with 10/20 mm spans at 0.5 mm/min using the electromechanical test frame. Typically, three to four test specimens were utilized at each indentation load. In addition, a series of indentations with different indent loads ranging from 100 N to 700 N were made in air for 20 s on 2 mm-thick soda-lime glass slides by using silicon nitride ball projectiles. Related crack systems were characterized in size and configurations. This was done to acquire implications of indentation cracking in silicon nitride targets by silicon nitride ball indentation, based on the fracture pattern and/or formations of multiple surface/subsurface crack systems generated in glass that would be easily observable due to its transparency. Results on soda-lime glass will be presented and described in Appendix.

Results and Discussion

Post-Impact Strength

The results of strength testing for impacted AS800 target specimens are depicted in figure 3, where individual values of post-impact flexure strength were plotted as a function of impact velocity for different projectile materials. As-received flexure strength (“AS”) of AS800 was included for comparison. The strength data on hardened steel ball projectiles that were determined previously [18] were also included. Many of specimens impacted at low velocities ≤300 m/s with metallic projectiles did not incur fractures originating from the impact sites. Those specimens not failing from fractures initiating at the impact sites were equivalent in strength to the corresponding as-received specimens. The “zero” strength

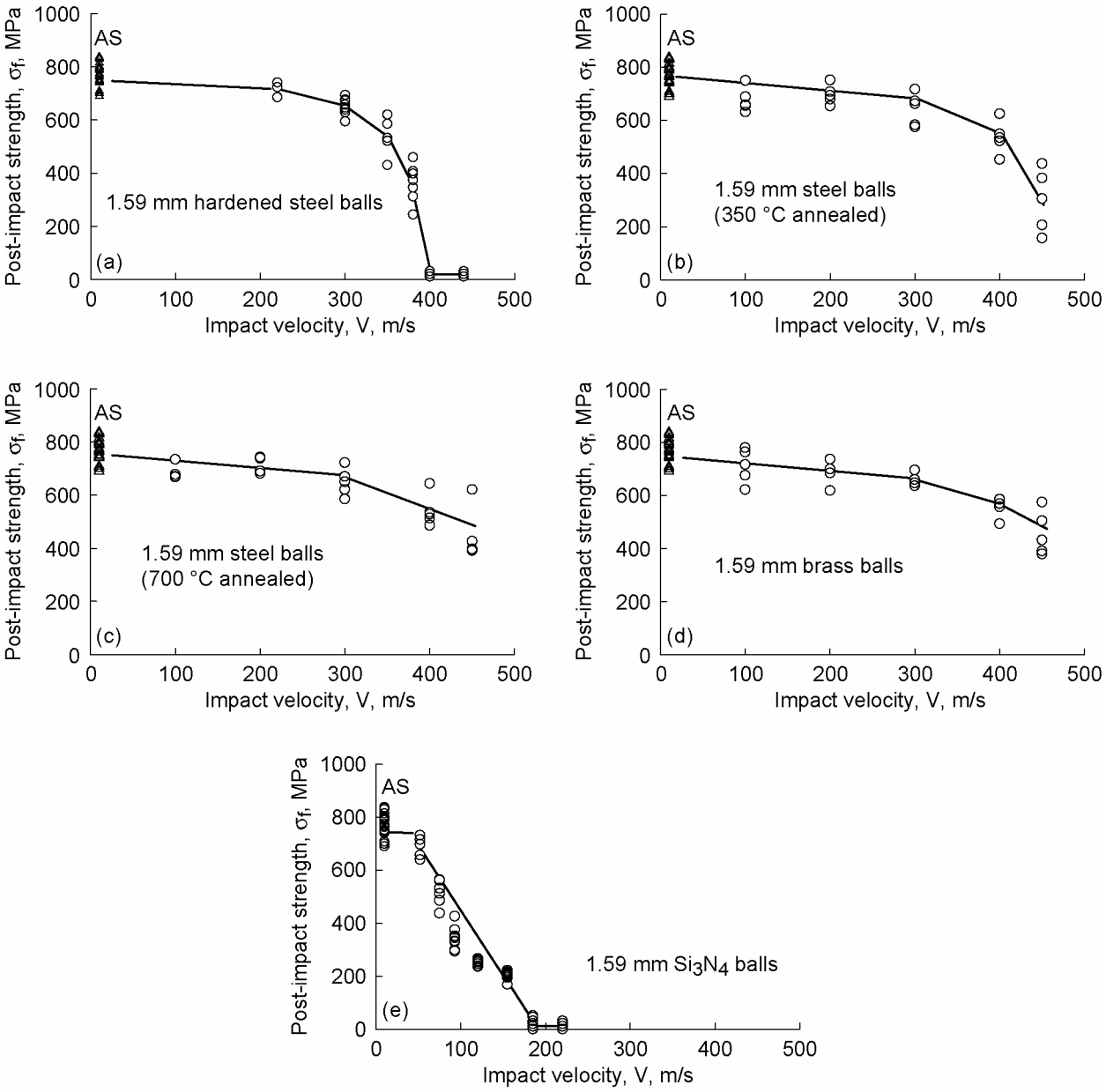

Figure 3.—Post-impact strength as a function of impact velocity, determined for AS80 silicon nitride flexure target flexure specimens impacted by 1.59-mm diameter ball projectiles of different materials at ambient temperature. (a) Hardened steel ball projectiles [18]; (b) steel ball projectiles annealed at 350 °C; (c) steel ball projectiles annealed at 700 °C; (d) brass ball projectiles; and (e) silicon nitride ball projectiles. "AS" stands for as-received strength.

shown for hardened steel ball and silicon nitride ball projectiles in the figure represents the specimens fractured upon impact, where the impact force was sufficient to break test specimens into two pieces, with failure originating from the impact site. This velocity has been defined as a "*critical impact velocity* (V_c)" in our previous work [17–20].

Figure 4 shows a summary of post-impact strength as a function of impact velocity with the five different projectile materials simplified from the data in figure 3, in which average strength was now used to better represent and compare the degree of FOD damage among different projectiles. Strength degradation with regard to the "as-received" strength was evident with increasing impact velocity for all

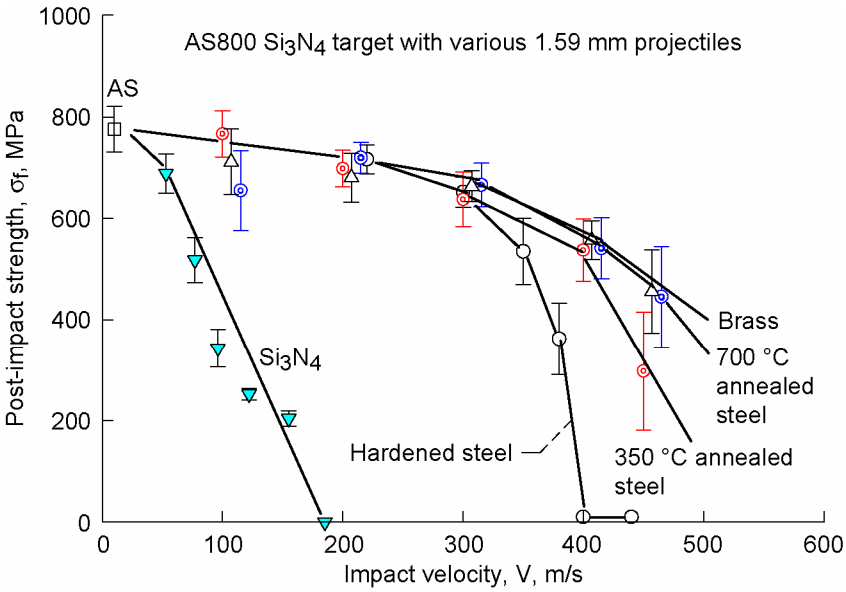

Figure 4.—Average post-impact strength of AS800 silicon nitride flexure target specimens as a function of impact velocity, impacted with 1.59 mm-diameter ball projectiles of different materials at ambient temperature.

the projectiles used. For the metallic projectiles, corresponding post-impact strength for a given impact velocity at ≥300 m/s was a function of material's hardness. The least strength degradation occurred in the soft brass projectiles with hardness of H_v = 1.9 GPa (see table 1); whereas, the greatest strength degradation occurred in the hardened steel ball projectiles with hardness of H_v = 8.2 GPa. However, of the five projectile materials, the greatest strength degradation took place with the silicon nitride ball projectiles, where strength degradation started even at very low impact velocity of 50 m/s and a critical impact velocity was only 180 m/s. Hence, for a given silicon nitride target material, the value of hardness of a projectile would be the most important factor to affect the severity of localized impact damage. One might consider elastic modulus of projectile to be another important factor. However, this cannot be supportive if one considers that elastic modulus of steel projectiles was all consistent with a value of about 200 GPa, independent of annealing temperature (see table 1).

From figure 4, the critical impact velocity can be readily determined for hardened steel and silicon nitride ball projectiles. However, the critical impact velocity could not be determined easily for annealed steel ball (350 and 700 °C) and brass ball projectiles, due to the limit of the current FOD test rig in achieving higher impact velocities ≥ 500 m/s. Approximated critical impact velocities were determined alternatively by the extrapolation of the data in figure 4 for annealed steel and brass ball projectiles. The critical impact velocities for all projectiles thus determined are:

V_c = 400 m/s: hardened steel balls
$V_c \approx$ 500 m/s: steel balls annealed at 350 °C
$V_c \approx$ 600 m/s: steel balls annealed at 700 °C
$V_c \approx$ 600-700 m/s: brass balls
V_c = 180 m/s: silicon nitride balls

A summary of critical impact velocity as a function of hardness of projectile materials is shown in figure 5. Despite the prediction of V_c made for some projectiles, the overall curve fitting was very reasonable to get a relationship between V_c (in m/s) and H_v in (GPa)

$$V_c \approx -33.7H_v + 700 \quad (1)$$

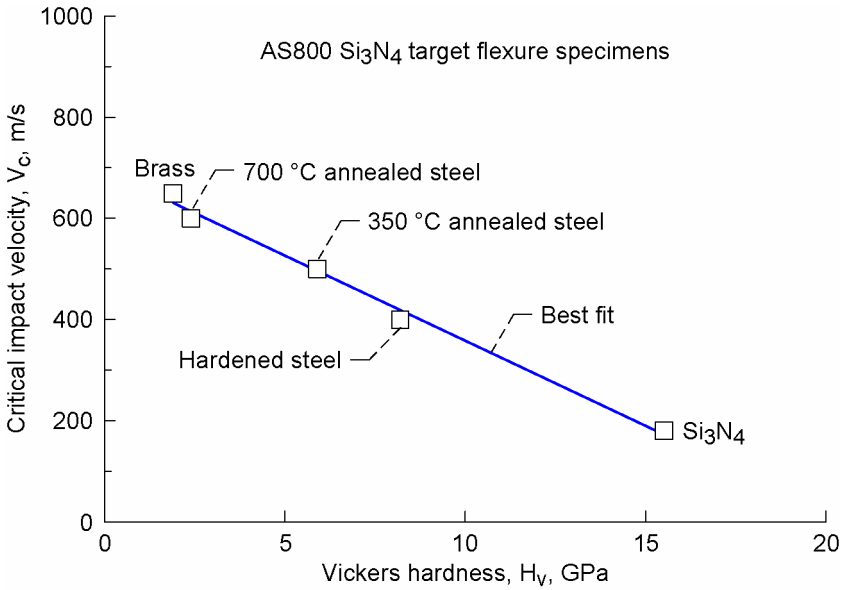

Figure 5.—Critical impact velocity as a function of hardness of 1.59 mm-diameter ball projectiles of different materials, impacted on AS800 silicon nitride flexure target specimens at ambient temperature.

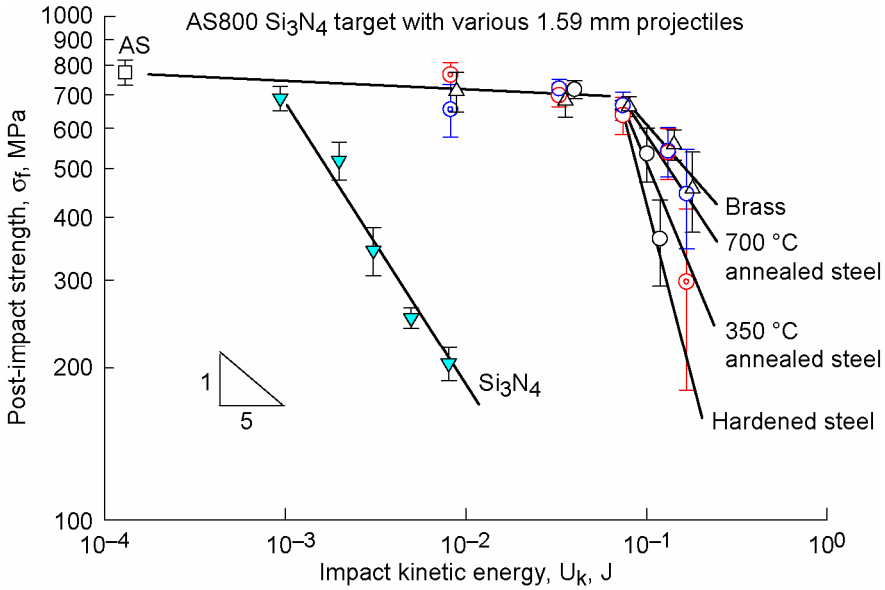

Figure 6.—Post-impact strength as a function of impact kinetic energy for AS800 silicon nitride flexure target flexure specimens, impacted with 1.59 mm-diameter ball projectiles of different materials.

for $H_v \geq 2$ GPa. This implies that hardness of projectiles is a key material parameter to affect most the critical impact velocity for a given target material/specimen configuration.

Figure 6 shows a summary of post-impact strength as a function of impact kinetic energy (U_K). Again, significant strength degradation occurred at much lower kinetic energy with the silicon nitride projectiles, as compared with the metallic projectiles. For the metallic projectiles, strength degradation occurring in a narrow range of kinetic energy depends on hardness of projectile materials at a given

kinetic energy. A model on strength degradation by spherical projectiles has been proposed with several assumptions and its resulting post-impact strength (σ_f) is expressed [1]

$$\sigma_f = \Phi(k/E)^{2/15} R^{-1/15} K_{Ic}^{4/3} \; U_K^{-1/5} \tag{2}$$

$$U_K = \frac{1}{2} m V^2 \tag{3}$$

where Φ is a constant, and k is a Poisson's ratio- and elastic-modulus dependent parameter, E is elastic modulus of target material, R is the radius of projectile, K_{Ic} is fracture toughness of target material, and m is the mass of projectile. For a given target material and a given material and geometry of a projectile, the post-impact strength depends on $U_K^{-1/5}$. It is noted from the figure that discrepancy in slope between the prediction (= –1/5) and the experimental data was significant, particularly for the metallic projectiles. The discrepancy is thought to be attributed to two plausible factors: (1) significant plastic deformation of a projectile upon impact, which might invalidate the model's assumption of idealized elastic impact, and (2) formation of well-developed cone cracks, which is a basis of equation (2), might not have always occurred; ring cracks and/or any other complex damage might have independently or simultaneously occurred so that a formation of one singular crack system could not be expected to occur for a wide range of impact velocity. Impact morphology will be discussed in the next section. A somewhat reasonable agreement for the silicon nitride projectiles indicates that the impact event between AS800 targets and Si_3N_4 ball projectiles could be characterized as one governed primarily by elastic-elastic impact with a presumably consistent crack configuration. Finally, it should be noted that post-impact strength or FOD was not solely influenced by the impact momentum (= mV) or impact energy (U_k) but by projectile hardness, keeping in mind that even if the silicon nitride projectile has less than half the mass of steel or brass projectile, it still created for a given impact speed much more damage than any other metallic projectiles.

Impact Morphology

A summary of impact morphologies of projectiles and their respective impact sites is summarized in figure 7. The metallic ball projectiles were flattened or severely deformed upon impact as a result of accompanying plastic deformation. At higher impact velocities (>300 m/s), the hardened steel projectiles were subjected to extreme heat evidenced by burning marks or fractured into several pieces. By contrast, other metallic ball projectiles, annealed steel or brass projectiles, did not fracture but were subjected to continuous flattening up to 450 m/s, as seen from the figure (also see their side-views). For a given impact velocity, the degree of flattening was dependent on material's hardness. The silicon nitride ball projectiles were intact up to 100 m/s but shattered or pulverized above 100 m/s, as shown in the figure.

Impact sites of target specimens were characterized with material transfer from the metallic projectiles to the target specimens, due to an instantaneous 'cold welding' effect, see figure 7. This material transfer, of course, was more significant at higher impact velocity (>300 m/s) than lower impact velocity. In post-impact strength testing, failure of specimens impacted by metallic projectiles at velocities below the "critical impact velocity" commonly originated from ring cracks. The failure path in this case was straight and cut through the boundary of the intermediate damage zone. Well-developed cone cracks were observed in specimens impacted at velocity close to and above the "critical impact velocity" in which target specimens fractured into two pieces upon impact. Detailed descriptions on impact morphology of AS800 impact sites by hardened steel ball projectiles can be found elsewhere [18, 19]. Radial cracks emanated from the impact sites of specimens impacted by silicon nitride ball projectiles at 200 m/s, as shown in figure 7, which was responsible for significant strength degradation.

Projectile material	Impact part	Impact velocity			
		100 m/s	200 m/s	400 m/s	450 m/s
Hardened steel	Impact site				
	Projectile		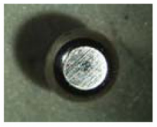		
Steel 350 °C annealed	Impact site				
	Projectile		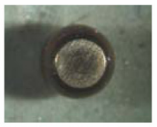	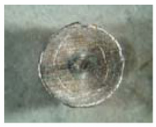	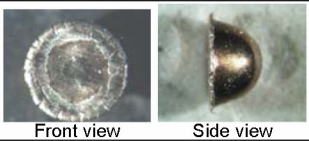 Front view Side view
Steel 700 °C annealed	Impact site				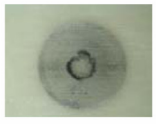
	Projectile				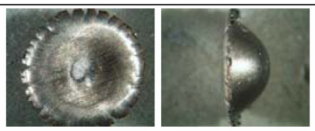 Front view Side view
Brass	Impact site				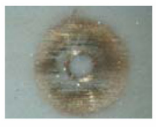
	Projectile	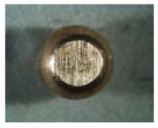		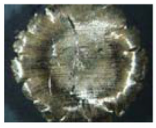	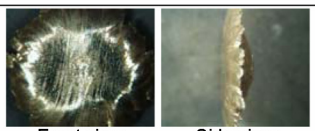 Front view Side view
Ceramic (Si_3N_4)	Impact site		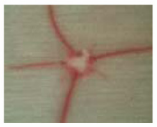	—	—
	Projectile			—	—

Figure 7.—A summary of impact morphologies of target impact sites and ball projectiles used in FOD testing. Note that the side views of steel ball projectiles annealed at 350 and 700 °C and brass ball projectiles, impacted at 450 m/s, are also included.

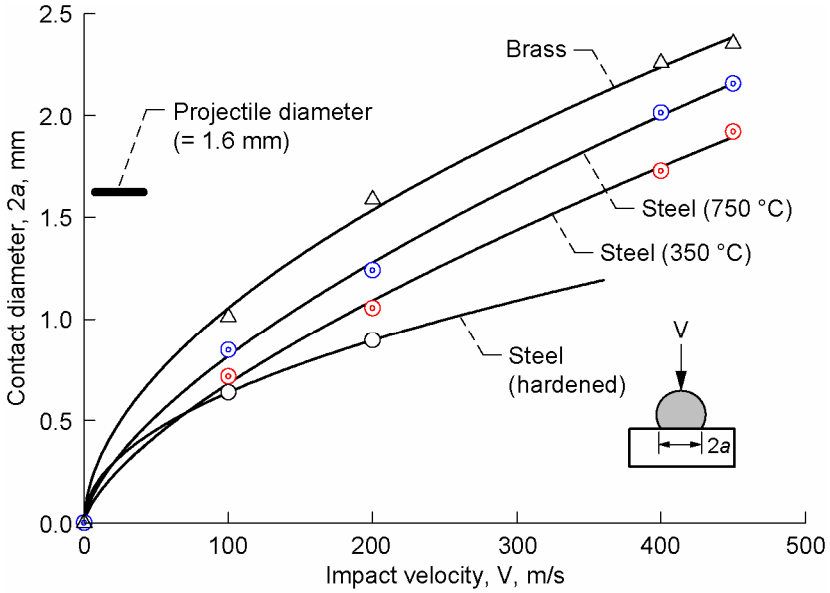

Figure 8.—Contact diameter as a function of impact velocity, impacted onto AS800 silicon nitride by different metallic projectiles.

An effort to collect projectiles upon impact, as mentioned in the Experimental Procedures section, was made to gather information on the degree of their impact plastic deformation. Figure 8 shows the results of measurements of contact diameter of flattened metallic projectiles, as a function of impact velocity. For a given impact velocity, contact diameter was in descending order from brass to annealed steel to hardened steel ball projectiles. This indicates clearly that hardness was a key parameter to the degree of plastic deformation of metallic projectiles upon impact.

Comparison With Sharp SiC Particle Impact

A comparison of post-impact strength of silicon nitrides subjected to a single impact event with 1.59-mm-diameter ball projectiles (this study) and a sharp SiC-particles (grit nos. 16 and 46) multiple impact [3, 30] is depicted in figure 9. Considerable strength degradation occurred in the case of sharp particle impact even at much lower impact kinetic energy, showing that the severity of impact damage was far greater in “sharp” particle impact than in “blunt” ball projectile impact. The sharp particle impact typically produced radial cracks emanating from the impact sites, similar to the Vickers indent cracks that originate from the corners of an impression site, thereby resulting in significant strength degradation. It should be noted that fracture toughness of AS440 silicon nitride was not significantly different from that of AS800 but greater (about 30 percent) than that of GN10 or SN220 silicon nitride. Figure 10 shows a typical impact morphology of a SN220 silicon nitride target showing radial cracks emanating from the impact site with no. 16 sharp SiC particle impacted at 80 m/s [30]. The comparison in figure 9 concludes that for a given target and impact energy, FOD of brittle materials depends on not only the material but the geometry of projectiles, as also mentioned previously [18, 19].

Static Indentation Responses

Impression Responses of Metallic Projectiles

The static indentation experiments with metallic ball projectiles on an AS800 silicon nitride disk showed that a flattened circular area of contact—a sign of plastic deformation—was well developed on

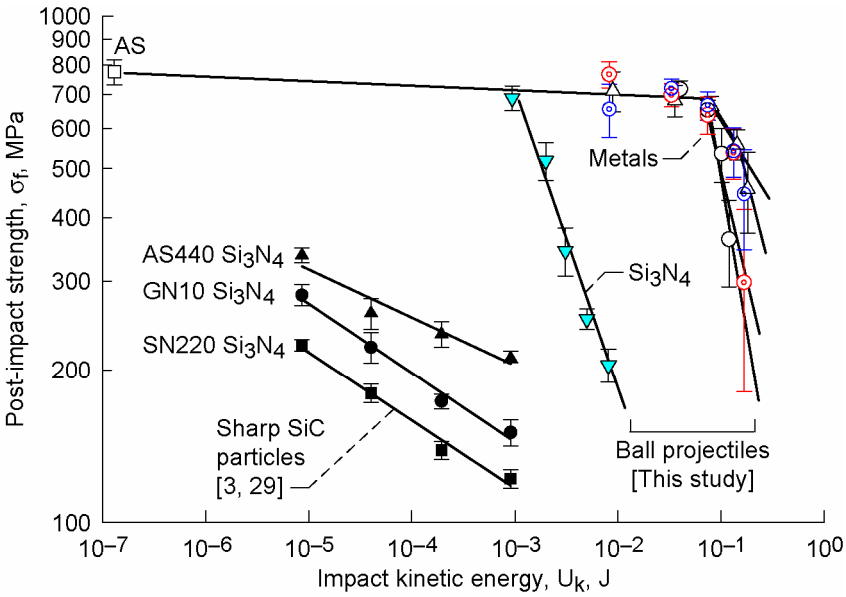

Figure 9.—Comparison in post-impact strength as a function of impact kinetic energy between ball projectiles [this study] and sharp SiC particles [3, 30] at ambient temperatures. Targets: AS800 silicon nitride for this study; three different silicon nitrides (AS440, GN10 and SN220) from the previous study [3, 29].

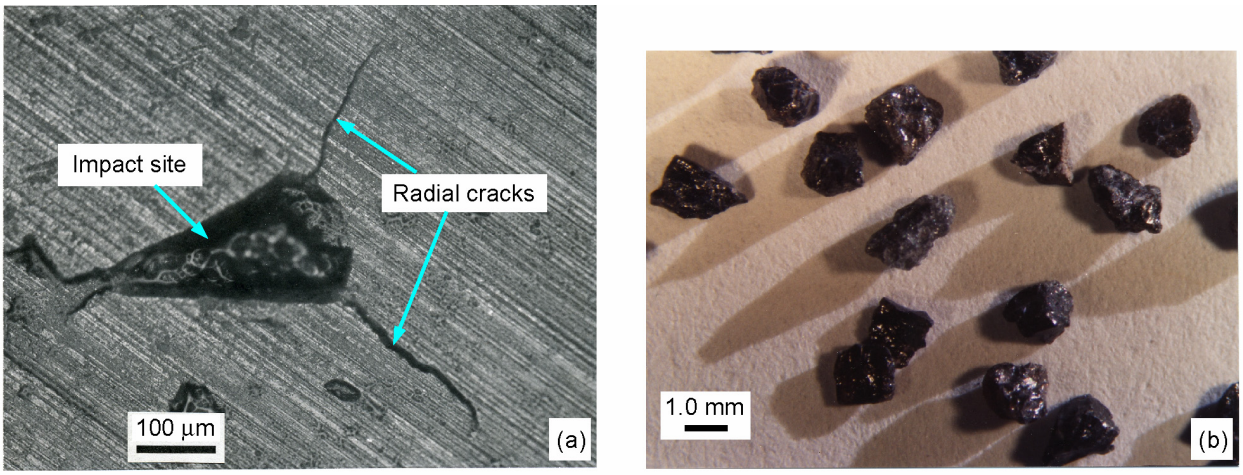

Figure 10.—(a) Typical morphology of impact site of a SN220 silicon nitride target specimen impacted by #16 SiC particle at 80 m/s in ambient-temperature air, and (b) SiC particles used [30].

each ball indenter, and as expected its circular impression size depended on applied indent load. No visible sign of cracking in contact area in the AS800 disk was observed even with the hardened steel ball projectile up to the maximum applied indent load of 3000 N. At 3450 N, the hardened steel ball failed in a mode of splitting into two pieces, as shown in figure 11, probably an evidence of tensile fracture due to a Poisson's effect.

The results of static indentation experiments are shown in figure 12, where contact impression diameter *d* was plotted as a function of applied static indent load *P*. For a given indentation load, the softer projectile yields the greater contact diameter, and *vice versa*. A similarity exists between the static

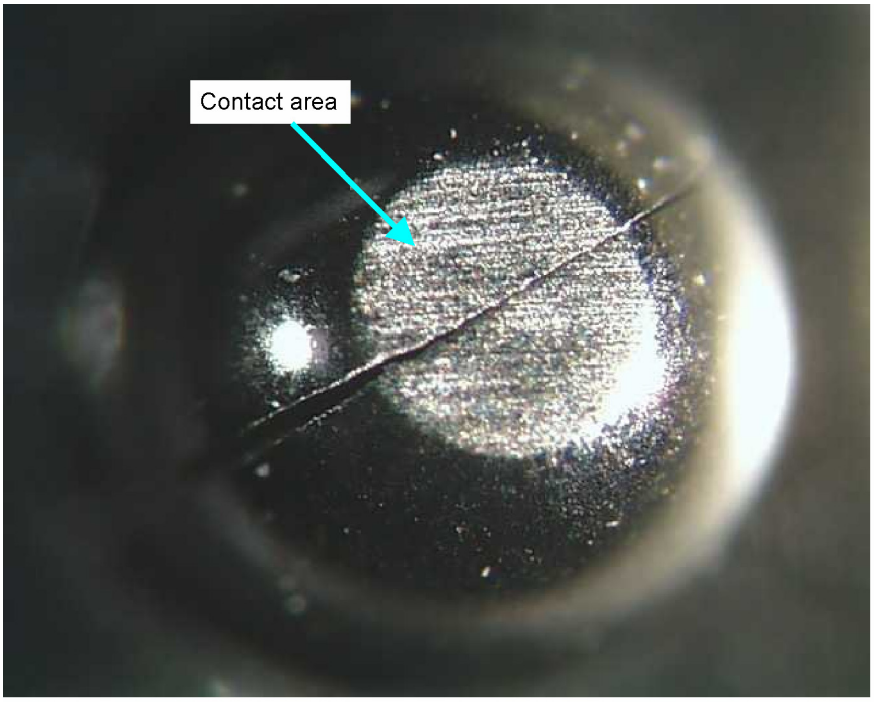

Figure 11.—Typical failure pattern of a 1.59 mm-diameter hardened steel ball projectile subjected to static indentation against an AS800 silicon nitride specimen. Note the flattened area of contact. Failure load = 3450 N.

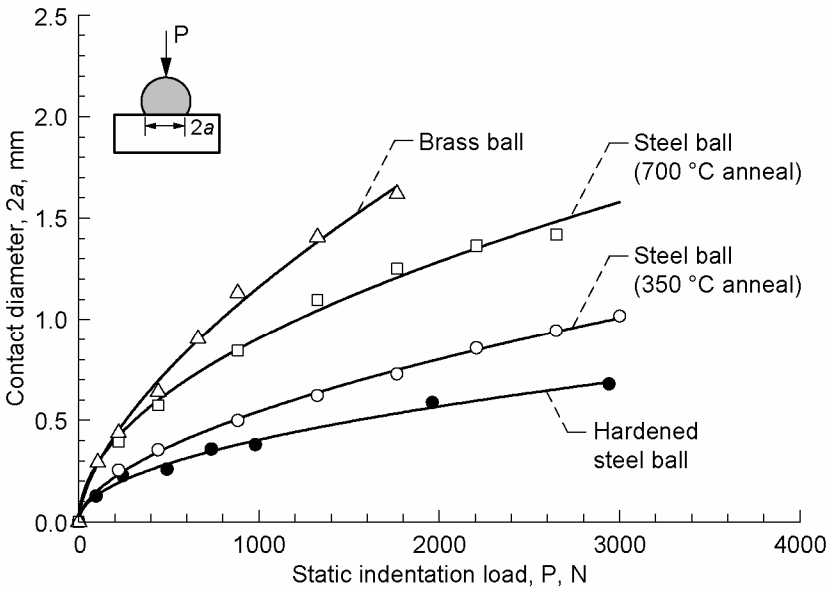

Figure 12.—Contact diameter as a function of static indentation load for AS800 silicon nitride by 1.59 mm-diameter metallic ball projectiles.

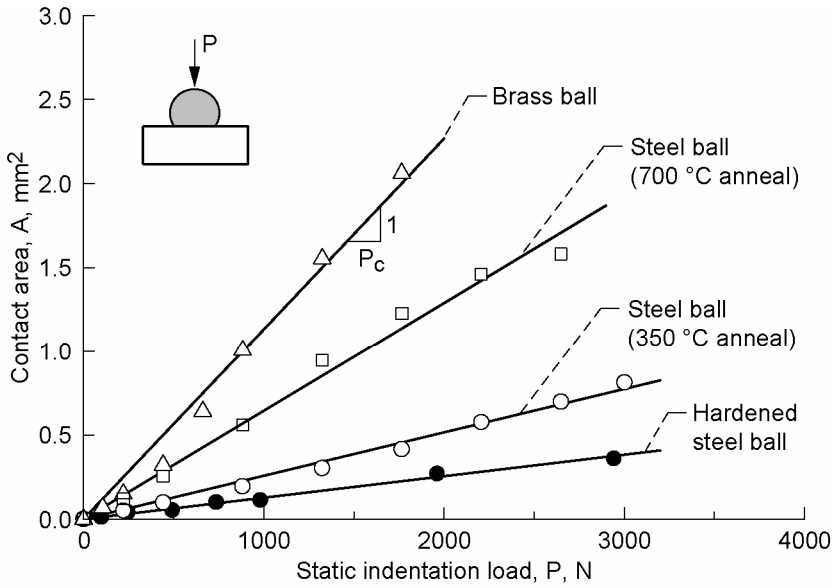

Figure 13.—Contact area as a function of static indentation load for AS800 silicon nitride by 1.59 mm-diameter metallic ball projectiles, plotted from the data in Figure 12.

indentation results of figure 12 and the dynamic impact results of figure 8, indicative again of hardness or ductility of projectile materials being a key material parameter to affect the degree of ball projectile deformation and consequently FOD behavior. Also, from figures 8 and 12, an important implication can be drawn such that a possible relation, although quasi-static, could be made between impact velocity and static indentation load, from which impact load could be estimated, which is a subject of the next section. An alternative plot to the results of figure 12, contact area *versus* indent load, is presented in figure 13. This figure shows a well-defined linear relationship between contact area (A) and indent load (P) for all the metallic ball projectiles used. Hence, the slope of each line represents the inverse of contact pressure (compressive stress) such that

$$\frac{A}{P} = \frac{1}{p_c} \tag{4}$$

where p_c is contact pressure or contact compressive stress. The fact that for a given projectile material the slope was constant indicates that yield or flow stress of each metallic ball projectile would be constant, regardless of the degree of plastic deformation. As a consequence, all the metallic projectiles could be considered to have acted as rigidly-perfectly plastic at least in response to ball projectile indentation against AS800 target silicon nitride. The values of contact pressure or yield stress of projectile materials determined based on equation (4) with the experimental data through a functional fit are shown in table 2.

TABLE 2.—VALUES OF AVERAGE COMPRESSIVE CONTACT PRESSURE (P_C) ESTIMATED FROM FIGURE 13 BASED ON EQ. (4).

Ball projectile material	Average compressive contact pressure (p_c) or compressive yield stress (MPa)
Hardened steel ball	7816±1064
350 °C annealed steel ball	3872±75
700 °C annealed steel ball	1549±41
Brass ball	882 ±30

Static Indentation Response of Target to Silicon Nitride Ball Projectiles

Crushing strength of silicon nitride ball.—Projectiles crushing strength (load), determined with a total of seven silicon nitride ball projectiles, was found to be 1735±125 N. Note that this crushing load of ceramic ball projectiles was lower than that (= 3450 N) of hardened steel ball projectiles. Some of significant Herzian contact stresses and contact size at fracture can be estimated using the following formulae [31]

$$\sigma_{\max}^{p} = \chi_1 \left[\frac{P}{K_D^2 \, C_E^2} \right]^{\frac{1}{3}} \tag{5}$$

$$\sigma_r = \frac{1-2\nu}{3} \sigma_{\max}^{p} \tag{6}$$

$$a = \chi_2 [P K_D C_E]^{\frac{1}{3}} \tag{7}$$

where $\sigma_{\max}^{p}$, σ_r, and a are the maximum compressive contact stress, the maximum radial tensile stress at the circular boundary of the surface of contact, and the contact radius, respectively. K_D is a geometry dependent parameter and C_E depends on Poisson's ratio and elastic modulus. χ_1 and χ_2 are numeric constants. Use of the crushing test configurations and crushing load (= 1735 N) gives rise to the values of

$$\sigma_{\max}^{p} \approx 25 \; GPa$$

$$\sigma_r \approx 3.8 \; GPa$$

$$a \approx 180 \; \mu m$$

The calculated value (= 180 μm) of contact radius was in reasonable agreement with that (= 210 μm) observed from a ceramic ball projectile subjected to an indent load of 1700 N, where the ball still survived. However, both the magnitudes of $\sigma_{\max}^{p}$ and σ_r were far greater than the compressive (≈ 10 GPa)[1] and tensile (≈900 MPa) strengths of the Si_3N_4 ball projectile material. This would impose a difficulty as to which stress has caused the failure of the ceramic balls in crushing testing. More detailed information on stress distributions through the body of a ball is needed to better understand the failure source in ball crushing.

Fracture of ceramic ball projectiles was typified with several broken fragments in a splitting mode of failure by tensile stress, in principal similar to failure of hardened steel balls. A typical example of a crushed ceramic ball is shown in figure 14. Shape of fragments each representing a wedge toward the center of the ball is indicative of a role of tensile stress in fracture.

Indentation strength response.—Indentation strength of AS800 flexure specimens indented with 1.59-mm-diameter silicon nitride ball indenters is shown in figure 15. Strength degradation started at an indent load of 500 N and increased with further increasing indent load. This threshold indent load where strength degradation initiated was much greater than that (≤ 10 N) of sharp Vickers indentation [17]. Note that the maximum indent load applied was 1700 N, which was close to the average crushing strength

[1]The compressive strength of ceramics has been known to be typically 10 times the tensile strength for a first-order approximation. Hence, the estimated compressive strength of the ceramic ball projectile would be around 10 GPa, based on the tensile strength data (>900 MPa) shown in table 1.

Figure 14.—A typical failure pattern of a 1.59 mm-diameter silicon nitride ball indenter subjected to crushing testing against AS800 silicon nitride flexure specimen; Crushing load = 1690 N.

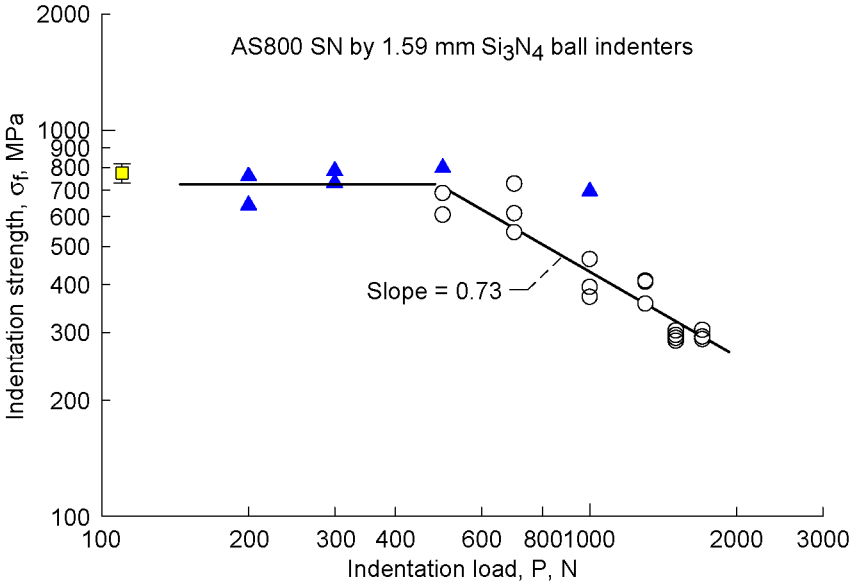

Figure 15.—Indentation flexure strength of AS800 silicon nitride flexure specimens as a function of indentation load, indented with 1.59 mm-diameter silicon nitride ball indenters. AS: as-received strength. The closed triangle symbols represent flexure specimens not fractured from indents.

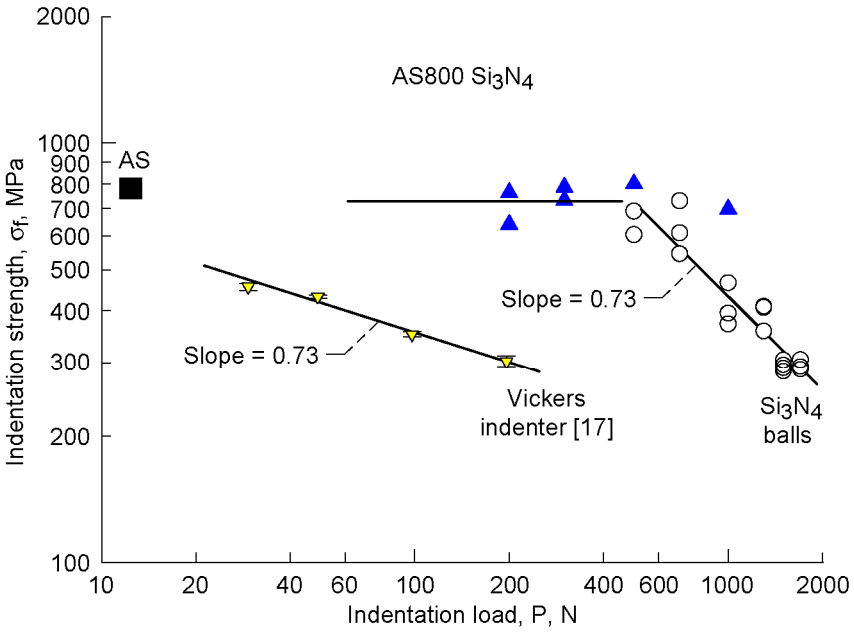

Figure 16.—Comparison of indentation strength of AS800 silicon nitride in flexure between 1.59 mm-diameter silicon nitride ball indenters and Vickers diamond indenter [17].

of the silicon nitride balls. At 1700 N, well-developed cone cracks were evident from the fracture surfaces of strength-tested specimens. Figure 16 compares the indentation strengths of AS800 flexure specimens between silicon nitride ball indenters and Vickers diamond indenter [17]. Significant strength degradation occurred for Vickers indentation even at lower indent loads, since strength-controlled radial cracks were readily developed even at lower indent loads in Vickers indentation. By contrast, less strength controlling ring type of cracks or cone cracks were typified for silicon nitride ball indentation. This response of indentation strength to 'blunt' ball indenter versus 'sharp' Vickers indenter is very much analogous to that of post-impact strength to ball projectile versus SiC sharp particle impact (see fig. 9). The best fit equations in figure 16 are:

$$\log \sigma_f = -0.730 \log P + 4.822 \tag{8}$$

$$\log \sigma_f = -0.227 \log P + 3.001 \tag{9}$$

for silicon nitride ball and Vickers indentations, respectively. The respective coefficients of correlation (r_{coef}) in the fit were 0.9406 and 0.9899. Note that the slopes in the fit are quite different: –0.73 versus –0.23, indicative of difference in crack configurations between the two indenters. The degree of strength scatter for both cases is also noted.

In order to determine contact (or ring crack) sizes produced on both AS800 flexure specimens and ceramic ball indenters, additional tests were conducted for polished AS800 flexure specimens in a range of indentation loads from 100 to 1700 N using each individual ball indenter for each given indentation. Typically, one to three indentations were made for a given indentation load. The results are shown in figure 17. No ring crack or any visible damage was developed at indent loads below 500N, in which no strength degradation occurred, as also seen from figure 15. At ≥500 N, the ring crack sizes increased with increasing indent load. It was generally observed that the ring cracks generated at contact sites at low

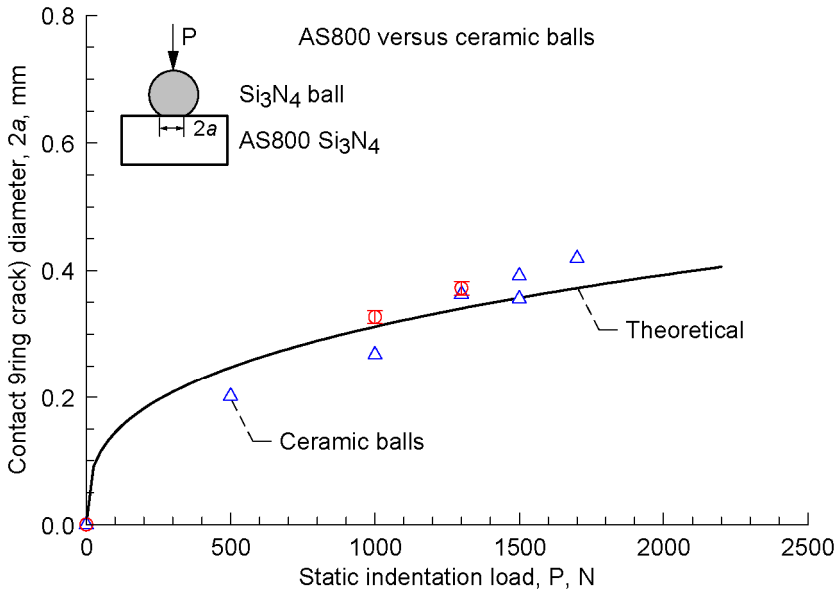

Figure 17.—Size of ring cracks as a function of indentation load on AS800 silicon nitride flexure specimens indented by 1.59 mm-diameter silicon nitride ball indenters. Triangle symbols represent for cracks on ceramic ball indenters and circle symbols represent for cracks on AS800 flexure specimens.

indent loads were of shallow depth but that well-defined cone cracks extended deeper through the material body with significant depth with increasing indent load. Radial racks, responsible for significant strength degradation, were not seen from AS800 specimen optically even at the highest indent load of 1700 N. It is also noted from figure 17 that the contact sizes calculated based on equation (7) were in good agreement with the experimental data. This concludes that the contact size for a given indent load approximately corresponded to ring crack size, which indicates that the tensile stress, greater than the material's strength, occurred along the circular boundary of the surface of contact thus to produce the ring crack, as predicted from equation (6) [31]. With a continuous loading sequence, a series of concentric ring cracks can be formed. Detailed examination of indent morphologies, using an appropriate means such as SEM, is also needed. Typical optical images of contact sites of both silicon nitride ball indenter and its mating surface of AS800 silicon nitride flexure specimen are shown in figure 18. Formations of a ring crack on the indenter and a somewhat featureless impression on the AS800 surface are noted.

To better understand indentation responses to silicon nitride ball indentation, soda-lime glass slides were alternatively used to determine associated indentation strength and contact sizes. The results, comparison and brief discussion can be found in the appendix.

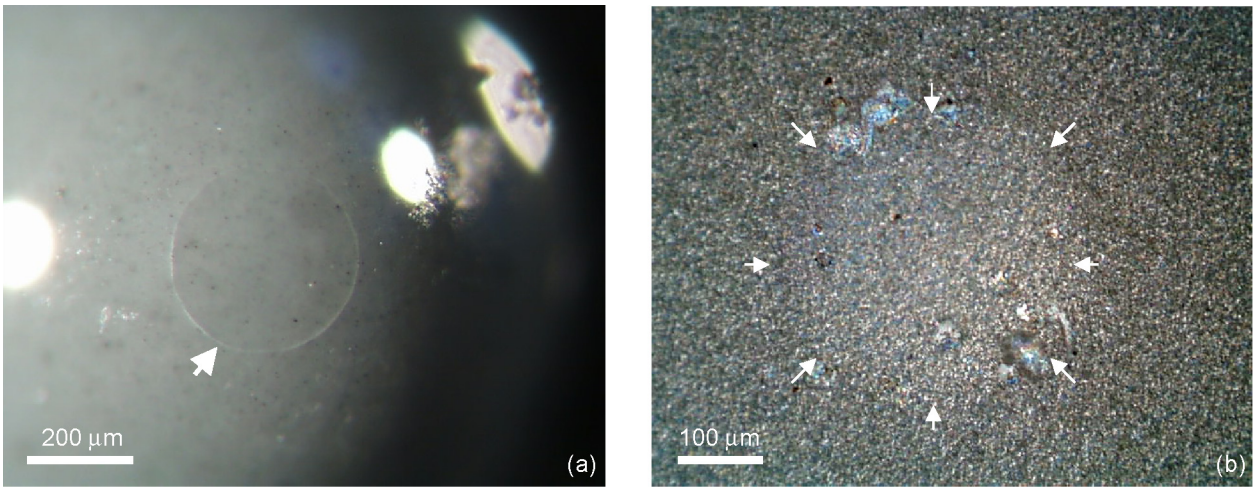

Figure 18.—Typical optical appearances of contact sites on: (a) 1.59 mm-diameter silicon nitride ball indenter showing a ring crack (arrowed); and (b) mating AS800 silicon nitride flexure surface (arrowed), indented at 1500 N.

Estimation of Impact Load

A prediction of quasi-static impact load could be made by using the static and impact plastic deformation (contact diameter) data (figs. 8 and 12) of metallic projectiles and the static indentation and post-impact strength data of AS800 target specimens by silicon nitride projectiles (figs. 3 and 15). The procedure as to how to predict impact load is illustrated in figure 19, starting from the impact associated data, correlating them to the static associated data, and then finding the quasi-static impact load. Analytically, both the data in figures 8 and 12 and those in figures 3 and 15 can be formulated through functional-fit regression analyses to obtain a final form of impact load as a function of impact velocity:

$$P_i = \alpha\ V^{\beta} \tag{10}$$

where P_i is predicted impact load. The estimated parameters α and β are listed in table 3 for all five different projectiles. A summary of the predicted impact load using the parameters is presented in figure 20. This figure also includes the predictions based on the simplified quasi-static, elastic impact model previously suggested, which is expressed as reference 1

$$P = \Phi'(k/E)^{-2/5}\rho^{3/5}R^2V^{6/5} \tag{11}$$

where Φ' is a constant and ρ is the density of projectile. As can be seen from the figure, reasonable agreement between the data and theory was found for the hardened steel ball and ceramic ball projectile, particularly at lower impact velocity. However, there was significant deviation from the theory for the softer metallic projectiles. Note that the model does not incorporate the effect of hardness so if there is predominant plasticity in impact event, the experimental data would be expected to deviate from the theoretical prediction.

Although the above approach to predict quasi-static impact load based on both plasticity and indent strength data would be seemingly reasonable particularly at low impact velocity at which the overall geometry of metallic projectiles would not change significantly upon impact, it is still an approximation and therefore must be validated with actual impact load measurements. This experimental work requires a series of records of force and deformation in response to a specific impact event. This work would be the next task of future FOD studies. Also, additional future work may include impact modeling, effect of projectile size and its geometry, and effect of protective coatings, etc.

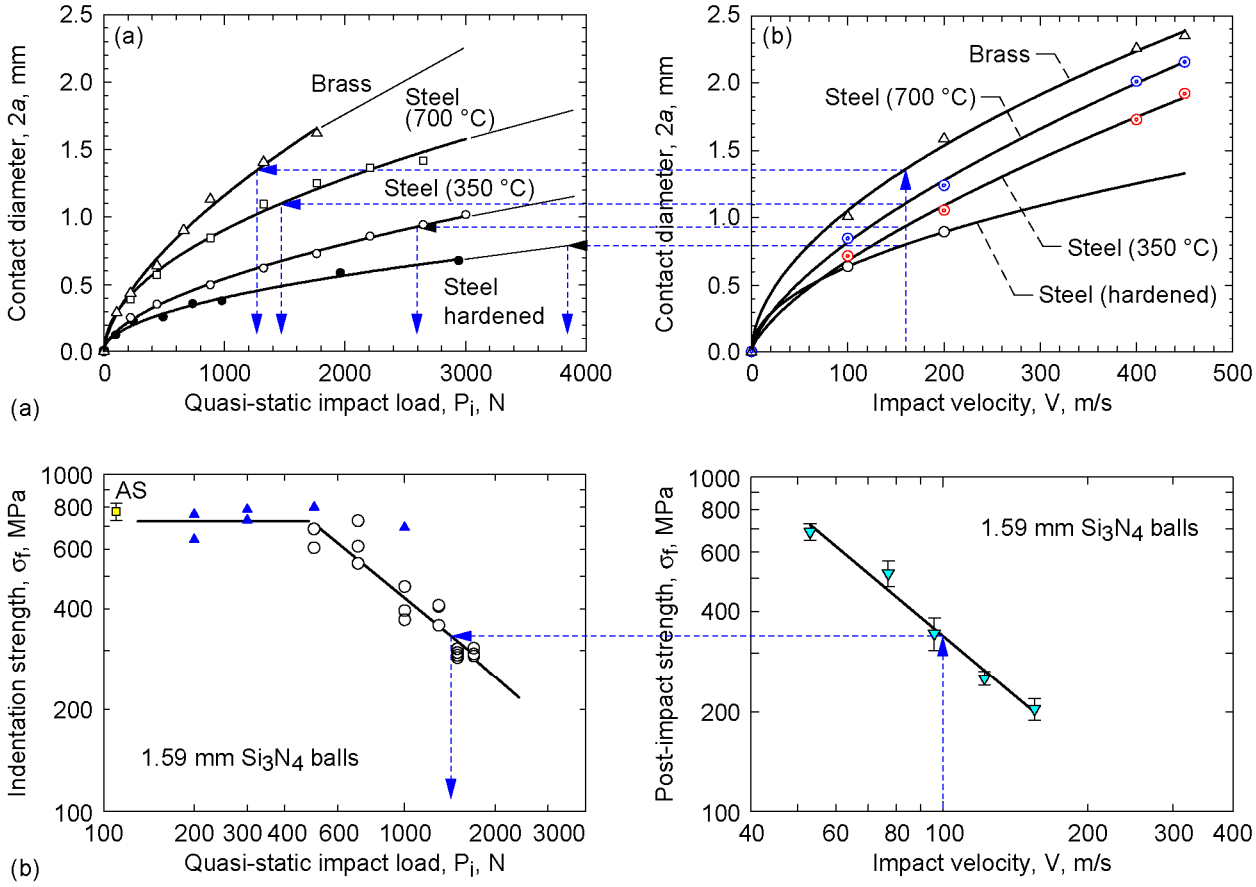

Figure 19.—Illustrations of the prediction of quasi-impact load based on static and impact related data for: (a) metallic ball projectiles; and (b) silicon nitride ball projectiles. Note that the label "Static indentation load, P" in Figures 12 and 15 was replaced with "Quasi-static impact load, P_i" for prediction purpose. Steps (1) through (4) for prediction procedure are also indicated.

TABLE 3.—PARAMETERS IN P_I-V RELATION IN EQUATION (10) FOR ESTIMATION OF QUASI-STATIC IMPACT LOAD

Projectiles (1.59 mm diameter)	Parameters in P_i-V relation	
	α	β
Hardened steel balls	26.4	0.99
350 °C annealed steel balls	5.7	1.21
700 °C annealed steel balls	2.3	1.28
Brass balls	15.9	0.87
Silicon nitride balls	0.73	1.64

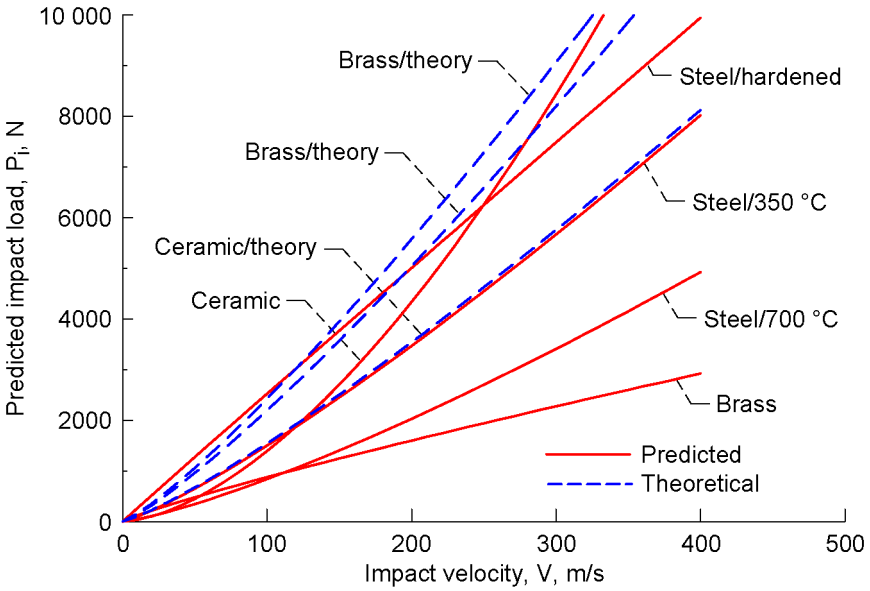

Figure 20.—Prediction of quasi-static impact load for different projectile materials. Theoretical prediction based on Eq. (11) is also included.

Conclusions

(1) The overall impact damage of AS800 silicon nitride was found to be greatest with silicon nitride ball projectiles. Of the metal projectiles, impact damage including post-impact strength and projectile deformation was lowest, intermediate and greatest, respectively for brass, 700 °C annealed steel, 350 °C annealed steel, and hardened steel ball projectiles.

(2) For metal projectiles, the key material parameter to affect most FOD behavior was hardness of projectile materials. The critical impact velocity was correlated with hardness of projectile materials.

(3) Prediction of impact load based on the projectile's plasticity and target's strength data obtained from both impact and static events seemed to be reasonable, although they are to be validated by a more rigorous experimental approach.

Appendix

Results on Soda-Lime Glass With 1.59 mm-diameter Silicon Nitride Ball Indenters

Contact Size Data on Soda-Lime Glass

Soda-lime glass slides, measuring 75, 25, and 1.0 mm, respectively, in length, width, and thickness, were used to determine contact (ring crack) data as a function indentation load at ambient temperature in air. The maximum indent load sustainable by the glass slides was found to be 700 N. At an indent load of 10 N, a series of faint concentric ring cracks formed. This pattern of cracking developed further into more significant ring/cone cracking as indent load increased. Typical indent patterns showing those ring/cone cracks are shown in figure A1. At a higher indent load of 700 N, some less-defined radial cracks developed at just outside the contact region. Figure A2 shows the results of the determinations of sizes of the contact regions including inner and outer ring cracks (d_i and d_o) and the size of bottom cone diameters (D). Theoretical contact size based on equation (7) is included and agrees well with the data on inner ring crack sizes (d_i). For comparison, the data on AS800 silicon nitride in figure 17 are also included in the figure. The theory seemed to agree well with both glass and silicon nitride material data when d_i was taken as a value of contact diameter.

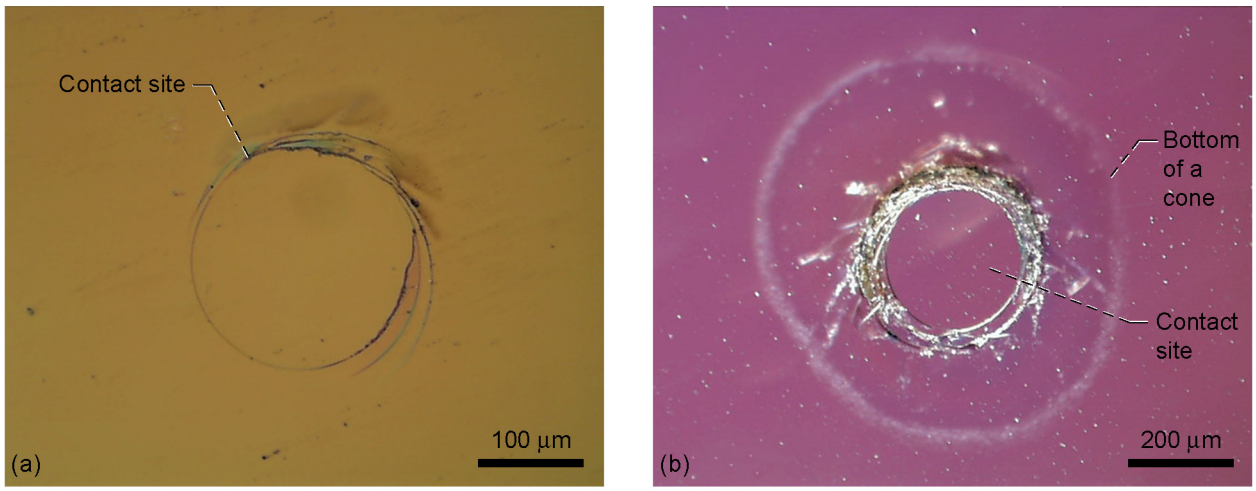

Figure A-1.—Typical examples of contact surfaces of soda-lime glass slides indented with 1.59 mm-diameter silicon nitride ball indenters: (a) indent load 100 N, and (b) indent load 700 N.

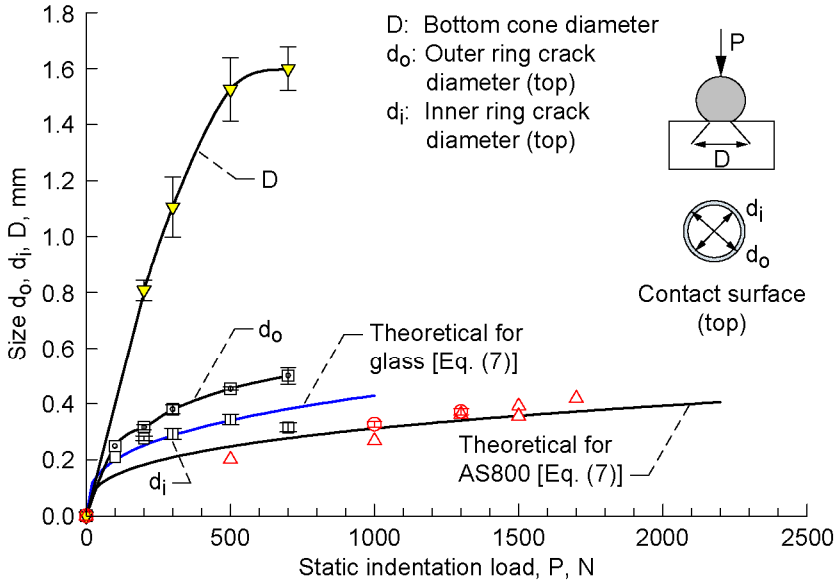

Figure A-2.—Contact size and cone crack size data determined for soda-lime glass slides indented with 1.59 mm-diameter silicon nitride ball indenters. Theoretical contact diameter based on Eq. (7) is included. Also, the data on AS800 silicon nitride in Figure 17 is included for comparison.

Indentation Strength Data on Soda-Lime Glass

Indentation strength of the soda-lime glass slides indented with 1.59 mm silicon nitride ball indenters was determined in ambient-temperature air in 20/40 mm span four-point flexure. Three indent loads of 100, 200, and 300 N were employed through a Zwick indenter on the glass slides at ambient temperature in air. An electromechanical test frame (Model 8562, Instron, Canton, MA) was used in strength testing under displacement control at a test rate of 0.5 mm/min. Three specimens were used at each indent load. The results are presented in figure A3. Scatter in data was significant, which indicates that increased number of test specimens would be a prerequisite. This ball indentation data was compared in the figure with Vickers indentation strength data determined previously [32]. The degree of indentation damage was evident between the two different indenters, again an issue regarding “sharp” versus “blunt” indentation. The best-fit equations in figure A3 were found to be

$$\log \sigma_f = -0.316 \log P + 2.500; \quad r_{coef} = 0.698 \tag{A1}$$

$$\log \sigma_f = -0.300 \log P + 2.176; \quad r_{coef} = 0.987 \tag{A2}$$

respectively, for silicon nitride ball and Vickers indenters. Figure A4 compares the indent strength data for AS800 flexure specimens (fig. 15) and soda-lime glass slides. The extent of strength degradation with respect to indent load differs for each type of indentation, although strength controlling flaws were considered to be cone type cracks, regardless of the type of indentation.

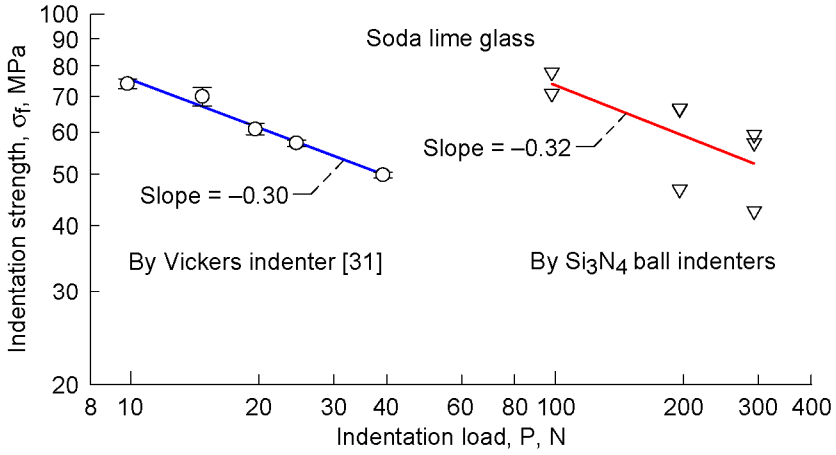

Figure A-3.—Indentation strength as a function of indent load for soda-lime glass slides indented with 1.59 mm-diameter silicon nitride ball indenters. Indentation strength data by Vickers indentation for soda-lime glass slides [31] is also included for comparison.

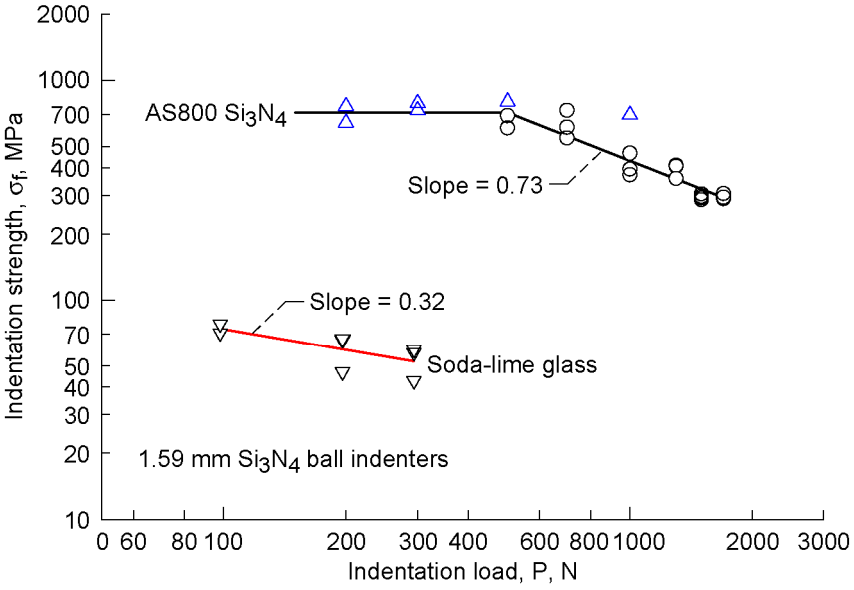

Figure A-4.—Comparison of indentation strength between AS800 silicon nitride flexure specimens and soda-lime glass slides, both indented with 1.59 mm-diameter silicon nitride ball indenters.

References

1. Wiederhorn, S.M. and Lawn, B.R., 1977, "Strength Degradation of Glass Resulting from Impact with Spheres," J. Am. Ceram. Soc., **60**[9–10], pp. 451–458.
2. Wiederhorn, S.M. and Lawn B.T., 1979, "Strength Degradation of Glass Impact with Sharp Particles: I, Annealed Surfaces," J. Am. Ceram. Soc., **62**[1–2], pp. 66–70.
3. Ritter, J.E., Choi, S.R., Jakus, K, Whalen, P.J., and Rateick, R.G., 1991, "Effect of Microstructure on the Erosion and Impact Damage of Sintered Silicon Nitride," J. Mater. Sci., **26**, pp. 5543–5546.
4. Akimune, Y., Katano, Y., and Matoba, K, 1989, "Spherical-Impact Damage and Strength Degradation in Silicon Nitrides for Automobile Turbocharger Rotors," J. Am. Ceram. Soc., **72**[8], pp. 1422–1428.
5. Knight, C.G., Swain, M.V., and Chaudhri, M.M., 1977, "Impact of Small Steel Spheres on Glass Surfaces," J. Mater. Sci., **12**, pp. 1573–1586.
6. Rajendran, A.M., and Kroupa, J.L., 1989, "Impact Design Model for Ceramic Materials," J. Appl. Phys, **66**[8], pp. 3560–3565.
7. Taylor, L.N., Chen, E.P., and Kuszmaul, J.S., 1986 "Microcrack-Induced Damage Accumulation in Brittle Rock under Dynamic Loading," Comp. Math. Appl. Mech. Eng., **55**, pp. 301–320.
8. Mouginot, R. and Maugis, D., 1985, "Fracture Indentation beneath Flat and Spherical Punches," J. Mater. Sci., **20**, pp. 4354–4376.
9. Evans, A.G. and Wilshaw, T.R., 1977, "Dynamic Solid Particle Damage in Brittle Materials: An Appraisal," J. Mater. Sci., **12**, pp. 97–116.
10. Liaw, B.M., Kobayashi, A.S., and Emery, A.G., 1984, "Theoretical Model of Impact Damage in Structural Ceramics," J. Am. Ceram. Soc., **67**, pp. 544–548.
11. van Roode, M., et al., 2002, "Ceramic Gas Turbine Materials Impact Evaluation," ASME Paper No. GT2002–30505.
12. Richerson, D.W. and Johansen, K.M., 1982, "Ceramic Gas Turbine Engine Demonstration Program," Final Report, DARPA/Navy Contract N00024–76–C–5352, Garrett Report 21–4410.
13. Boyd, G.L. and Kreiner, D.M., 1987, "AGT101/ATTAP Ceramic Technology Development," Proceeding of the Twenty-Fifth Automotive Technology Development Contractors' Coordination Meeting, p.101.
14. van Roode, M., Brentnall, W.D., Smith, K.O., Edwards, B., McClain, J., and Price, J.R., 1997, "Ceramic Stationary Gas Turbine Development—Fourth Annual Summary," ASME paper no. 97–GT–317.
15. Akimune, T., Akiba, T., and Ogasawara, T., 1995, "Damage Behavior of Silicon Nitride for Automotive Gas Turbine Use when Impacted by Several Types of Spherical particles," J. Mater. Sci., **30**, pp. 1000–1004.
16. Yoshida, H., Kano, S., Hasegawa, Y., Shimamori, T., and Yoshida, M., 1996, "Particle Impact Phenomena of Silicon Nitride Ceramic," Philo. Magazine A, **74**[5], pp. 1287–1297.
17. Choi, S.R., Pereira, J.M., Janosik, L.A., and Bhatt, R.T., 2002, "Foreign Object Damage of Two Gas-Turbine Grade Silicon Nitrides at Ambient Temperature," Ceram. Eng. Sci. Proc., **23**[3], pp. 193–202.
18. Choi, S.R., Pereira, J.M., Janosik, L.A., and Bhatt, R.T., 2004, "Foreign Object Damage Behavior in Flexure Bars of Two Gas-Turbine Grade Silicon Nitrides," Mater. Sci. Eng., **A379**, pp. 411–419.
19. Choi, S.R., Pereira, J.M., Janosik, L.A., and Bhatt, R.T., 2004, "Foreign Object Damage in Disks of Gas-Turbine-Grade Silicon Nitrides by Steel Ball Projectiles at Ambient temperature," J. Mater. Sci., **39**, pp. 6173–6182.
20. Choi, S.R., Pereira, J.M., Janosik, L.A., and Bhatt, R.T., 2002, "Foreign Object Damage in Disks of Two Gas-Turbine Grade Silicon Nitrides by Steel Ball Projectiles at Ambient Temperature," NASA/TM—2003–212224, National Aeronautics & Space Administration, Glenn Research Center, Cleveland, OH.

21. Choi, S.R., Bhatt, R.T., Pereira, J.M., and Gyekenyesi, J.P., 2004, "Foreign Object Damage Behavior of a SiC/SiC Composite at Ambient and Elevated Temperatures," Proceedings of ASME Turbo Expo 2004, June 14–17, 2004, Vienna, Austria; ASME Paper No. GT2004–53910.
22. Choi, S.R., Racz, Z., Bhatt, R.T., Brewer, D.N, and Gyekenyesi, J.P., 2005, "Effect of Projectile Materials on Foreign Object Damage of a Gas-Turbine-Grade Silicon Nitride," Proceeding of ASME Turbo Expo 2005, June 6–9, 2005, Reno, NV; ASME Paper No. GT2005–68866.
23. ASTM C 1259, Test Method for Dynamic Young's Modulus, Shear Modulus, and Poisson's Ratio for Advanced Ceramics by Impulse Excitation of Vibration, *Annual Book of ASTM Standards*, *Vol. 15.01*, ASTM, West Conshohocken, PA (2002).
24. ASTM C 1327, Test Method for Vickers Indentation Hardness of Advanced Ceramics, *Annual Book of ASTM Standards*, *Vol. 15.01*, ASTM, West Conshohocken, PA (2002).
25. ASTM C 1161, Test Method for Flexural Strength of Advanced Ceramics at Ambient Temperatures, *Annual Book of ASTM Standards*, *Vol. 15.01*, ASTM, West Conshohocken, PA (2002).
26. ASTM C 1421, Test Methods for Determination of Fracture Toughness of Advanced Ceramics at Ambient Temperature, *Annual Book of ASTM Standards*, *Vol. 15.01,* ASTM, West Conshohocken, PA (2001).
27. Choi, S.R. and Gyekenyesi, J.P., (a) Elevated-Temperature "Ultra"-Fast Fracture Strength of Advanced Ceramics: An Approach to Elevated-Temperature "Inert" Strength, ASME J. Eng. Gas Turbines & Power, **121** (1999) 18–24; (b) 'Ultra'-Fast Strength of Advanced Structural Ceramics at Elevated Temperatures, pp. 27–46 in *Fracture Mechanics of Ceramics*, Vol 13, Edited by R.C. Bradt, D. Munz, M. Sakai, V.Ya. Shevchenko, and K.W. White, Kluwer Academic/Plenum Publishers, New York, NY (2002).
28. Choi, S.R. and Gyekenyesi, J.P., 2001, "Slow Crack Growth Analysis of Advanced Structural Ceramics under Combined Loading Conditions: Damage Assessment in Life Prediction Testing, ASME J. Eng. Gas Turbines & Power, **123** (2001) 277–287.
29. Choi, S.R. and Krause, D.L., "Assessments of Mechanical and Life Limiting Properties of Two Candidate Silicon Nitrides for Stirling Convertor Heater Head Applications," NASA/TM—2006-214089, National Aeronautics and Space Administration, Glenn Research Center, Cleveland, Ohio (2005).
30. Choi, S.R., Ritter, J.E., and Jakus, K., "Erosion and Impact Behavior of Various Advanced Ceramics at Ambient and Elevated Temperatures," unpublished work, University of Massachusetts, Amherst, MA (1988).
31. Timoshenko, S.P. and Goodier, J.N., Theory of Elasticity, Section 140, McGraw-Hill, Tokyo, 3rd Ed (1970).
32. Choi, S.R., unpublished work, National Aeronautics and Space Administration, Glenn Research Center, Cleveland, OH (1991).

REPORT DOCUMENTATION PAGE

Form Approved
OMB No. 0704-0188

1. AGENCY USE ONLY (*Leave blank*)	2. REPORT DATE	3. REPORT TYPE AND DATES COVERED
	September 2006	Technical Memorandum

4. TITLE AND SUBTITLE

Foreign Object Damage in a Gas-Turbine Grade Silicon Nitride by Spherical Projectiles of Various Materials

5. FUNDING NUMBERS

WBS–22–714–30–09

6. AUTHOR(S)

Sung R. Choi, Zsolt Racz, Ramakrishna T. Bhatt, and David N. Brewer

7. PERFORMING ORGANIZATION NAME(S) AND ADDRESS(ES)

National Aeronautics and Space Administration
John H. Glenn Research Center at Lewis Field
Cleveland, Ohio 44135–3191

8. PERFORMING ORGANIZATION REPORT NUMBER

E–15563

9. SPONSORING/MONITORING AGENCY NAME(S) AND ADDRESS(ES)

National Aeronautics and Space Administration
Washington, DC 20546–0001

10. SPONSORING/MONITORING AGENCY REPORT NUMBER

NASA TM—2006-214330

11. SUPPLEMENTARY NOTES

Sung R. Choi, University of Toledo, 2801 W. Bancroft Street, Toledo, Ohio 43606; Zsolt Racz, Ohio Aerospace Institute, 22800 Cedar Point Road, Brook Park, Ohio 44142; and Ramakrishna T. Bhatt and David N. Brewer, NASA Glenn Research Center. Responsible person, Ralph Pawlik, organization code RXL, 216–433–8563.

12a. DISTRIBUTION/AVAILABILITY STATEMENT

Unclassified - Unlimited
Subject Category: 07

Available electronically at http://gltrs.grc.nasa.gov

This publication is available from the NASA Center for AeroSpace Information, 301–621–0390.

12b. DISTRIBUTION CODE

13. ABSTRACT ***(Maximum 200 words)***

Assessments of foreign object damage (FOD) of a commercial, gas-turbine grade, in situ toughened silicon nitride ceramic (AS800, Honeywell Ceramics Components) were made using four different projectile materials at ambient temperature. AS800 flexure target specimens rigidly supported were impacted at their centers in a velocity range from 50 to 450 m/s by spherical projectiles with a diameter of 1.59 mm. Four different projectile materials were used including hardened steel, annealed steel, silicon nitride ceramic, and brass. Post-impact strength of each target specimen impacted was determined as a function of impact velocity to appraise the severity of local impact damage. For a given impact velocity, the degree of strength degradation was greatest for ceramic balls, least for brass balls, and intermediate for annealed and hardened steel balls. For steel balls, hardened projectiles yielded more significant impact damage than annealed counterparts. The most important material parameter affecting FOD was identified as hardness of projectiles. Impact load as a function of impact velocity was quasi-statically estimated based on both impact and static indentation associated data.

14. SUBJECT TERMS	15. NUMBER OF PAGES
Foreign object damage (FOD); Silicon nitride; Projectile materials	32
	16. PRICE CODE

17. SECURITY CLASSIFICATION OF REPORT	18. SECURITY CLASSIFICATION OF THIS PAGE	19. SECURITY CLASSIFICATION OF ABSTRACT	20. LIMITATION OF ABSTRACT
Unclassified	Unclassified	Unclassified	